IL NUOVO CIMENTO Vol. 27 C, N. 4 Luglio-Agosto 2004
DOI 10.1393/ncc/i2004-10033-y

UV meteor observation from a space platform

P. Scarsi(*)

INAF, Istituto di Astrofisica Spaziale e Fisica Cosmica, sez. Palermo - Palermo, Italy
AREA CNR - Via U. La Malfa 153, 90146 Palermo, Italy

(ricevuto il 12 Novembre 2004; approvato il 24 Novembre 2004)

Summary. — The paper reports on the evaluation of the meteor light curve in the 300–400 nm UV band produced by meteoroids and space debris interacting with the Earth atmosphere; the aim is to assess the visibility of the phenomenon by a near-Earth space platform and to estimate the capability for measuring the solid-body influx on the Earth from outer space. The simulations have been conceived on the basis of general processes only, without introducing *a priori* observational inputs: the calibration with real data can be made in orbit by validation with "characterized" meteor streams. Computations are made for different values of the entry velocity (12 to 72 km/s) and angle of impact of the meteoroid when entering the atmosphere, with initial-mass values ranging from 10^{-12} kg to the kg size encompassing the transition from micrometeorites ($m < 10^{-9}$–10^{-8}kg) to the "ablation" regime typical of larger masses. The data are presented using units in UV Magnitudo to facilitate direct comparison with the common literature in the field. The results concern observations of the atmosphere up to $M_{\rm UV} = 18$ by a height of 400 km above the Earth surface (average for the International Space Station—ISS), with reference to the mission "Extreme Universe Space Observatory—EUSO" designed as an external payload for the module "Columbus" of the European Space Agency. Meteors represent for EUSO an observable as a *slow* UV phenomenon with seconds to minutes characteristic time duration, to be compared to the *fast* phenomenon typical of the Extensive Air Shower (EAS) induced by the energetic cosmic radiation, ranging from microseconds to milliseconds. Continuous wide-angle observation by EUSO with its high inclination orbit and sensitivity reaching $M_{\rm UV} = 18$ will allow the in-depth exploration of the meteor "sporadic" component and to isolate the contribution of minor "streams".

PACS 96.50.Kr – Meteors, meteoroids, and meteor streams.
PACS 96.50.Mt – Meteorites, micrometeorites, and tektites.
PACS 95.55.Fw – Space-based ultraviolet, optical and infrared telescopes.

(*) E-mail: paolo.scarsi@pa.iasf.cnr.it

1. – Introduction

A "meteor" is the result of the interaction of a solid body ("meteoroid" or "space debris") with the air molecules and atoms when entering into the Earth atmosphere from outer space. The phenomenon is observable by the streak of light and the ionized trail produced along the trajectory of the body in its way down to the ground as a result of dissipation of the initial kinetic energy in the interaction processes.

The Earth atmosphere acts for the meteoroid as a dissipative medium as it does for the High Energy Cosmic Rays (HECR) which produce in the air a "particle shower avalanche effect" known as "EAS—Extensive Air Shower". Even though the mechanisms behind the energy release in the two processes are basically different, an observable result in both cases is the production of a fluorescence streak along the path of penetration in the atmosphere. "Meteors" and "EAS" can be observed in optical and UV from a space platform as tracks geometrically similar but strongly differentiated by the velocity of progression and the rate of variation of luminosity with track length. First evidence for the observation in UV of meteors from space has been obtained by the satellite "ARGO" [1].

Meteor investigation has produced a vast literature ranging from purely qualitative description to quantitative analysis and approach to the processes involved. A comprehensive review of the field can be found in [2]; the data reported have been obtained with different techniques (photon detection or radar sounding), lacking in general of inter-calibration and referring to observations made by ground-based or airplane-born instruments. Observations are mainly episodic both in space and time; the general picture and understanding currently accepted are largely dependent on the experimental conditions and on the models adopted. Usually the role of the upper atmosphere (above 300–400 km) is neglected and the "meteor region" is generically placed in the 100–200 km range above the Earth surface, with 100–120 km quoted as the conventional height for the maximum luminosity.

The mission "Extreme Universe Space Observatory—EUSO", conceived as an external payload for the European Space Agency (ESA) Module "Columbus" on the International Space Station—ISS, has been designed to measure the UV emission of the Extensive Air Shower (EAS) tracks [3]. Meteors are observed by EUSO, as a *slow* phenomenon with seconds to minutes characteristic time duration (propagation velocity $v < 72$ km/s), to be compared with the *fast* phenomenon typical of the EAS induced by energetic cosmic rays which ranges from microseconds to milliseconds ($v = 300000$ km/s). Because of its high sensitivity, EUSO will enable the extension of the range of observable meteors up to $M_{\mathrm{UV}} = 18$ from $M = 9$–10 typical of conventional ground and airplane observations and the limit value $M = 12$ obtained in a single dedicated observation with the 10 m Mt. Hopkins Telescope [4]. Due to their faint luminosity, micrometeoroids ($m < 10^{-9}$ kg) up to now accessible only by radar tracking or through direct recovery of the solid residual on the earth surface as "micro-meteorites", will be made accessible by EUSO to UV observation from space as "micro-meteors".

The systematic investigation from a space platform can overcome the major part of the difficulties of the ground-based experiments, such as the interference of the variable atmospheric transparency conditioning and the limitation of observations bound to a fix observational site.

The simulation program reported in this paper refers specifically to the observational conditions of EUSO; in this framework the aim is the evaluation of the light curve produced by meteoroids and space debris in the (300–400) nm UV band where EUSO

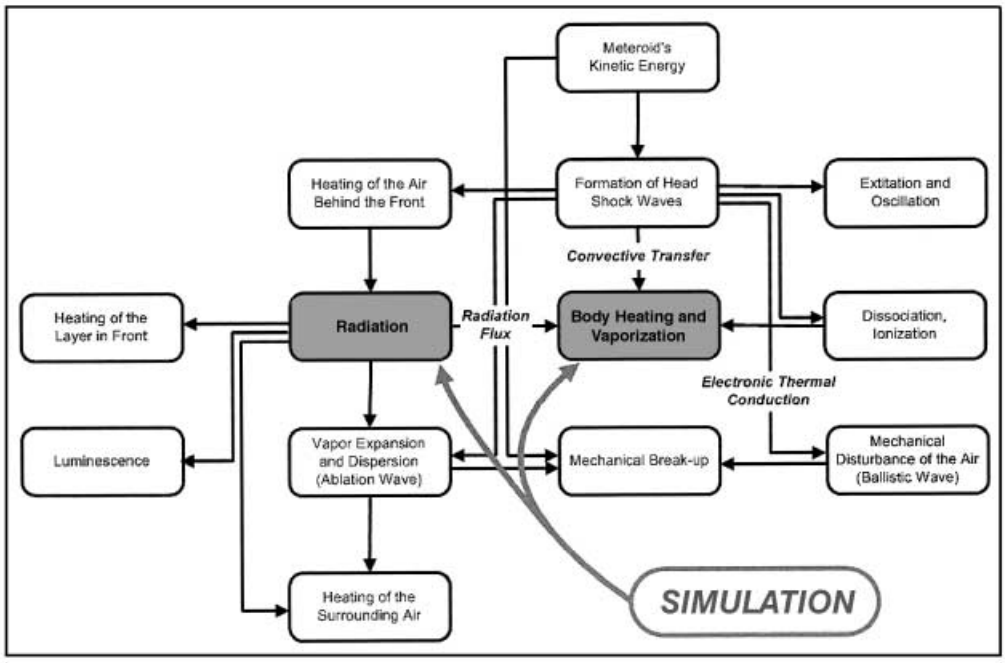

Fig. 1. – Energy conversion in meteor phenomena: after [5].

is sensitive. It has been conceived with a straightforward approach based on general processes, without *a priori* normalization to data from direct observations. A direct calibration can be made during the orbital operational life by validation with characterized meteor streams.

2. – Modeling. The meteor basic physical processes

The minimum velocity required to a meteoroid traveling in the interplanetary space to enter into the Earth atmosphere must be at least equal to the escape velocity $v_{\rm esc} = 11.2$ km/s for an object close to the Earth surface, corresponding to a kinetic energy of about $6 \cdot 10^7$ joule/kg. As the meteoroid is slowed down by friction with the air molecules, a complex series of processes occurs for the conversion of the meteoroid kinetic energy (fig. 1) [5]. The kinetic energy is partially converted into heat which in turn, if the mass exceeds a critical value of about $(10^{-8}– 10^{-9})$ kg for stony meteoroids, can vaporize by ablation the solid-body surface material and dissociate/ionize the surrounding atmospheric gas, with a process competing with the heat conduction to the inner body by leaving a steep temperature gradient; for mass values below this limit, heat propagation by conduction can prevail rising the temperature of the entire solid body to the melting point and preventing local ablation. For the mass interval approaching the critical value, a transition phase joins the two processes extreme.

Plank radiation emission by the solid body and by the vapors from ablation, together with the electronic transitions resulting from the excitation of the atoms involved (both from the atmosphere and the meteoroid) induce a luminous source which travels with the meteoroid. Taking into account the formation of shock waves produced in the air ahead of

the meteoroid, it is estimated that a fraction from 0.1 to 1 percent of the kinetic energy of the meteoroid is transformed into radiation in the optical-UV range. The "meteor visible flight" lasts few seconds when observed by standard Cameras (limit to 0 Magnitudo), Super-Schmidt Cameras (limit to Magnitudo 3) or Low Light Level Television (LLLTV) with sensitivity extending up to a Magnitudo about 9 [2]; the duration of the unobserved "dark flight" of the meteoroid can be substantially longer and may be traced by observing the emission at a higher level of sensitivity monitoring the phenomenon from space (EUSO limiting Magnitudo in UV reaches ≈ 18 when normalized to observations from ground in clear atmospheric conditions).

The basic assumptions adopted for the numerical simulation of the meteor light curve can be summarized in the following steps:

a) A numerical model for the Earth atmosphere extending to 900 km altitude above sea level to fully enclose the region of physical interest to the meteor phenomenon.

b) Geometry of a sphere for the meteoroid/debris entering the atmosphere and progressively slowed down by the drag due to the friction with the air molecules.

c) A simple model of the ablation process, which takes into account the progressive mass reduction of the body during its flight through the atmosphere as a result of sublimation of the outer layers resulting by the energy dissipation by heat production. The process considered is unique, without a distinct "preheating phase" as introduced by [2].

d) No fragmentation is considered.

e) The simulation computes the UV light curve converting and balancing the loss of kinetic energy into photon emission. The trajectory, speed and luminosity of the solid body is finally computed as a function of time.

3. – The Earth atmosphere

For meteor simulation, a profile of the Earth atmosphere is first required to provide a comprehensive set of values of temperature, pressure, density, absolute and cinematic viscosity, sound speed and molecular weight of the air as a function of altitude.

3˙1. *Homosphere.* – For the homosphere (the Earth atmosphere below 105 km altitude, where complete vertical mixing yields a near-homogeneous composition of about 78.1% N_2, 20.9% O_2, 0.9% Ar, 0.1% CO_2 and trace constituents) the USSA-76 (US Standard Atmosphere 1976) [6] has been adopted as a reference.

The model gives the temperature as a function of altitude calculated for piecewise linear temperature profile segments defined on the temperature gradients as showed in fig. 2. Air density and pressure have been then calculated by assuming the homosphere as a "perfect gas" of constant molecular weight $M = 28.964$ in hydrostatic equilibrium conditions function of altitude. For the parameters necessary in aerodynamic calculation, the following relations have been used:

$$a = 340.2941 \cdot \sqrt{\frac{T}{288.15}}\,, \tag{1a}$$

$$\eta = 1.702 \cdot 10^{-4} \cdot (1 + 3.29 \cdot 10^{-3} \cdot T + 7 \cdot 10^{-6} \cdot T^2)\,, \tag{1b}$$

where
a = speed of sound (m)$\cdot$ (s)$^{-1}$;
η = absolute viscosity (g) $\cdot$ (cm)$^{-1}\cdot$ (s)$^{-1}$;
T = temperature (K).

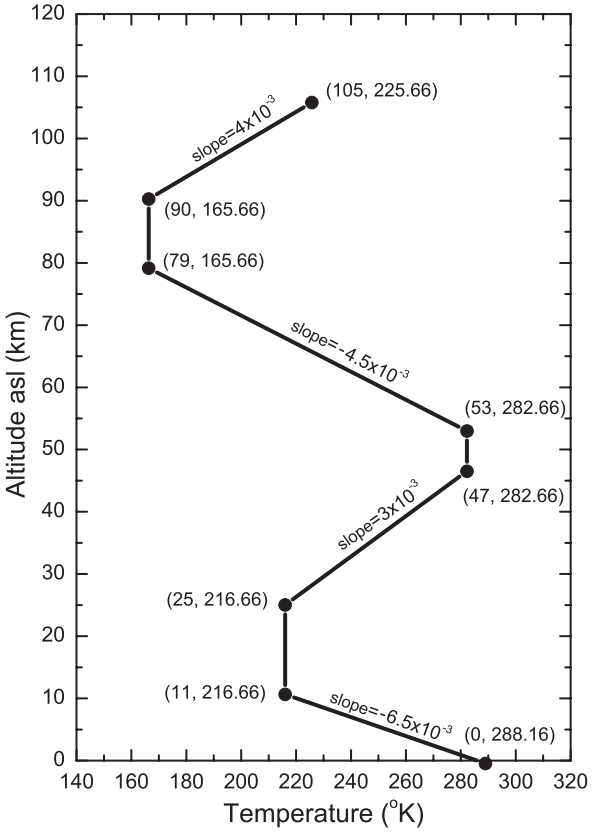

Fig. 2. – USSA-76, altitude *vs.* temperature profile (medium solar activity): after [6].

3˙2. *Heterosphere.* – For the heterosphere, from about 105 km up to the exosphere, (region where it can be assumed that the constituents are in diffusive equilibrium with no vertical mixing and the concentration profiles develop for each constituent independently under the influence of gravity and thermal diffusion), the Mass Spectrometer Incoherent Scatter MSISE-90 Atmosphere Model output data, as obtained for mean solar activity ($F_{10.7\text{avg}} = 140$) and daily mean geomagnetic index $A_p = 300$, have been adopted as ref. [7]. MSISE-90 determines temperature, density and number concentration of the major constituents up to exospheric altitudes as a function of the atmospheric state parameters (geodetic latitude, local solar time, universal time, geographic longitude, day of the year, daily solar flux index, mean solar flux index, daily mean geomagnetic index). The upper limit of the heterosphere (considered by enclosing the physical Earth Atmosphere as far as it is relevant in the meteor process) has been set at 900 km above the Earth surface. The MSISE-90 output data set has been divided into different altitude regions and the data points fitted in each interval with a high-order polynomial to obtain a continuous function for air temperature, pressure, density and molecular weight parameters as a function of altitude. For aerodynamic calculation in the rarefied atmosphere the mean free path length, the speed of sound and the dynamic viscosity have

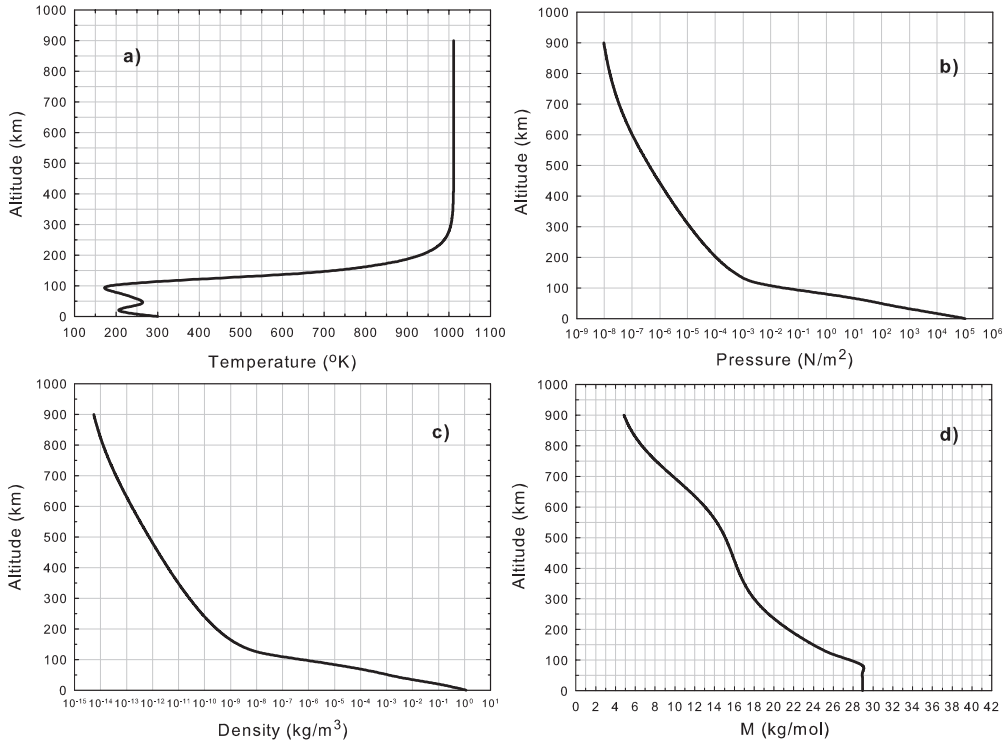

Fig. 3. – Altitude *vs.*: a) temperature, b) pressure, c) density and d) molecular weight. MSISE-90 after [7].

been approximated using the following relations:

$$L = \frac{\gamma \cdot T}{p \cdot \sqrt{2} \cdot \pi \cdot d_{\text{avg}}^2}\,, \tag{2a}$$

$$a = \sqrt{k \cdot \frac{p}{\gamma \cdot \rho}}\,, \tag{2b}$$

$$\mu = \frac{2}{3} \cdot L \cdot \rho \cdot a \cdot \sqrt{\frac{2}{\pi \cdot \gamma}}\,, \tag{2c}$$

where
L = mean free path of a molecule (m);
a = speed of sound (m)$\cdot$(s)$^{-1}$;
μ = dynamic viscosity (kg) $\cdot$ (s)$^{-1}\cdot$ (m)$^{-1}$;
γ = ratio of specific heats (= 1.44, in a nitrogen-dominated environment);
d_{avg} = mean collision diameter for nitrogen (= $3.62 \cdot 10^{-10}$(m));
k = Boltzmann constant (= $1.3807 \cdot 10^{-23}$ (J)$\cdot$ (K)$^{-1}$);
T = temperature (K);
p = pressure (N) $\cdot$(m)$^{-2}$.

Figures 3a, b, c, d show the values adopted for the relevant parameters used in the simulations as smoothed along the entire atmospheric depth considered.

4. – Motion of a spherical massive body in the atmosphere

The simulation program calculates position and velocity of the meteoroid in the atmosphere as a function of time in a bi-dimensional space, by using a Cartesian reference system with origin set at the Earth surface, in correspondence of the point of impact of the object in the atmosphere assumed at a given altitude (900 km) and with Y-axis directed towards Nadir; the meteoroid angle of entry is referred to the horizontal.

The deceleration equation assumes the momentum $m \cdot \mathrm{d}v$ lost by the meteoroid proportional to the momentum of the oncoming air flow, with the mass impinging upon a mid-sectional area S at velocity v in a time $\mathrm{d}t$ given by $S \cdot \rho \cdot v \cdot \mathrm{d}t$:

$$m \cdot \frac{\mathrm{d}v}{\mathrm{d}t} = -\Gamma \cdot S \cdot \rho \cdot v^2 \,, \tag{3}$$

where Γ is the drag coefficient, expressing the portion of the momentum of the oncoming flow that is converted into deceleration of the body. In aerodynamics, the drag coefficient is usually denoted by c_x or C_D, where $c_x = 2\Gamma$. The solid body is represented by a geometrical sphere (shape factor $A = 1.21$), with perfectly smooth surface and of homogeneous mass (no cracks or fractures weaken the solid-body structure); chemical and mineralogical composition of the meteoroid are not taken into account and a constant density is assumed. To simplify the model, neither fragmentation processes due to stress by high-speed impact with air molecules nor the deformation of the meteoroid during the flight in the atmosphere are taken into account and the body is considered self-similar during the meteor phenomenon, shape variation parameter μ constant and equal to $2/3$.

As far as the motion is concerned, the following constraints were adopted in the simulation of the atmospheric entry:

1. The meteoroid is traveling in a uniform gravitational field;
2. No correction is introduced for the Earth surface curvature, considered flat when comparing the Earth radius with the atmospheric thickness, nor for the atmosphere curvature at low entry angle values.
3. The spherical meteoroid is supposed to be a non-rotating object; such an assumption avoids a continuous correction in the direction of flight due to the Magnus effect (deviation in the direction of flight due to rotation on one of its axes).
4. For the aerodynamic force, no lift component is considered in the calculation (lift coefficient = 0.0).
5. Shock wave formation, as a first approximation, is not taken into account. Therefore a punctual determination of the local atmospheric parameters (air pressure, density and temperature) cannot be made during the meteor appearance; on the other hand, being mostly focused on the ablation phenomena and the emission of UV radiation, we can globally take into account shock wave effects by setting proper values for the heat transfer and the luminosity coefficients, which give an estimate on the sharing of the kinetic energy between thermal and luminous component.
6. For aerodynamic calculations, air molecules flow regime definition/transition during the meteoroid flight in the atmosphere is taken into account by a simple appropriate calculation of the drag coefficient (C_D). One assumes a strong Reynold number

(*Re*) dependence (*i.e.* air viscosity and density) of C_{D} at lower meteoroid velocity, while a Mach number (M) dependence is advocated for higher speed; different experimental datasets are used based on the different range of object velocity/fluid viscosity ratios. A high-order polynomial fitting procedure is then used to obtain a continuous function $C_{\mathrm{D}} = f\,(Re,\ M)$ and a numerical computation of C_{D} is made.

This approximation avoids the complication arising from to the fact that the transitional flow regime is not well understood and it is therefore difficult to cover the conditions from free-molecular flow to continuum flow (subdivided into incompressible, compressible transonic supersonic and hypersonic flow based on the Mach number) in a process anyway dominated by a large set of parameters.

5. – The ablation process

The mass-loss equation follows from the assumption that in the reference frame of the solid-body a portion Λ of the rate of the energy loss ($1/2 \cdot S \cdot \rho \cdot v^3$) of the oncoming stream of molecules is expended on the ablation (vaporization or fusion and spraying) of a mass $\mathrm{d}m$ in an interval time $\mathrm{d}t$. If ζ is the latent heat of vaporization or fusion of the meteoroid material in units of energy (including the energy that must be delivered to a mass $\mathrm{d}m$ in order to heat it from its initial temperature T_0 to its evaporation temperature), then the mass-loss equation takes the form

$$\frac{\mathrm{d}m}{\mathrm{d}t} = -\Lambda \cdot \frac{S \cdot \rho \cdot v^3}{2 \cdot \zeta}\,. \tag{4}$$

Some assumptions are made in order to simplify the modeling of the process:

1. The percentage of the total meteoroid kinetic energy (whose transformation is distributed according to a complex function of heating/ablation, radiation, ionization, fragmentation, shock waves, etc...) converted into thermal energy is considered constant during the meteoroid flight through the atmosphere. Namely, the kinetic energy converted into heat is assumed for each simulation run not to be a function of the meteoroid speed and mass and the heat transfer coefficient is maintained constant over the entire calculation.

2. In the ablation model considered, the heat generated by friction is initially deposited on the external surface of the solid and it propagates uniformly over the entire surface independently of the direction of flight. The heat is supposed to flow inward into the body with low efficiency (low thermal conductivity of the meteoroid) so that a steep temperature gradient is induced and only the outer husk melts. The resulting vaporized material is then removed by the air molecules flowing around the solid, exposing newer surface to the ablation process with a progressive reduction of the body mass and size.

3. No change in the mineralogical composition of the meteoroid is assumed as effect of the large amount of heat involved in the ablation process so that the density remains constant in the process.

5˙1. *Source of UV radiation for the "ablation process"*. – Starting point for the calculations is the assumption that a fraction of the meteoroid kinetic energy of the ablated material is converted into electromagnetic radiation [5] producing a source with visual luminosity L (W):

$$L = \tau \cdot \left(-\frac{\mathrm{d}m}{\mathrm{d}t}\right) \cdot \frac{v^2}{2}\,, \tag{5}$$

where τ is the dimensionless coefficient of efficiency for conversion into radiation of the kinetic energy of the vaporizing meteoroid material and $\mathrm{d}m/\mathrm{d}t$ is the instantaneous rate of ablation. We have assumed τ not to be a function of the speed and mass of the meteoroid and constant over each simulation run during the meteoroid flight in the atmosphere.

The following steps have been considered in the calculation of the UV radiation parameters:

1) The program calculates first the instantaneous visual luminosity L, then the optical flux density $F_d = L/4 \cdot \pi \cdot d^2 (\mathrm{W/m^2})$ as seen at the distance d of the meteor from an observer at ground in correspondence of the origin of the reference axes, and finally derives the value of the instantaneous meteor visual absolute magnitude M_{visual} by using the expression

$$M_{\mathrm{visual}} = -2.5 \cdot \log\left(\frac{F}{F_0}\right)\,, \tag{6}$$

where $F_0 = 3.38 \cdot 10^{-9}$ $(\mathrm{W/m^2})$ according to the calibration of Allen [8] is the visual flux density of a meteor with visual absolute magnitude $M = 0$ and $F = L/4 \cdot \pi \cdot 10^{10} (\mathrm{W/m^2})$ is the value of the of the visual flux density corresponding at the source with luminosity L as seen at the distance of 100 km from the observer at ground. It is customary in fact to express the visual magnitude of meteors in terms of an absolute magnitude M, the apparent magnitude as observed at 100 km [9].

To take into account the wavelength dependence of the meteors light flux, assumption on a particular meteor spectrum has to be made by setting a proper color index (*C.I.*) parameter and, assuming M_{visual} equal to M_{optical}, the absolute UV magnitude (M_{uv}) in the (300–400) nm range can be calculated by using the relation: $M_{(300\text{–}400\ \mathrm{nm})} = M_{\mathrm{optical}}$ – *C.I.* where $M_{(300\text{–}400\ \mathrm{nm})}$ is the UV absolute magnitude, M_{optical} is the optical absolute magnitude and *C.I.* is the color index. By adopting the *C.I.* "correction" parameter, even if in a very simplified way, the program can simulate emission of radiation from meteors with different composition, overcoming the fact that mineralogical/chemical meteoroid composition has not been taken into account for ablation.

2) In order to calculate the equivalent flux density S_ν in Jansky (1 Jansky = 10^{-26} watts/m^2/Hz) from the values of magnitudes at the effective wavelength λ_{eff}, the following relation has been used [8]:

$$S_\nu = A_\nu \cdot 10^{(-0.4 \cdot M_\nu)}\,, \tag{7}$$

where S_ν is the flux density in Jansky, M_ν is the meteor magnitude, A_ν is a constant; for meteor simulation values adopted are A_{uv}=1910 and A_{optical}= 3830, corresponding to the U and V filter, respectively.

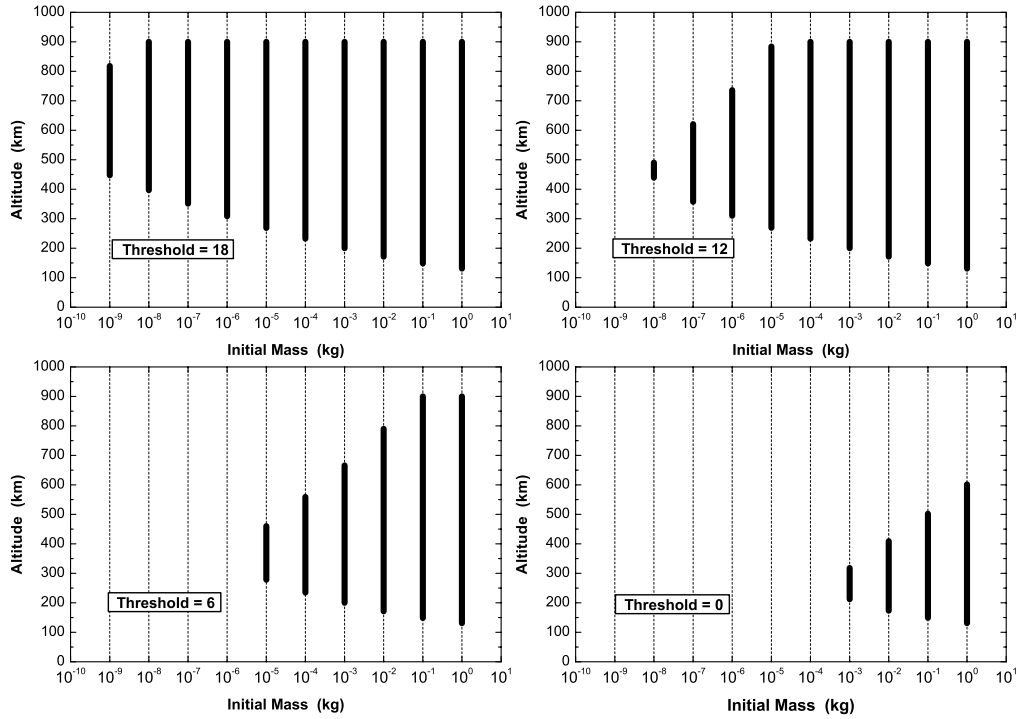

Fig. 4. – Start and end altitude for the observable meteor track as a function of the initial-mass value at various values of threshold for the UV-Magnitudo ("pure ablation process"; entry at 900 km with $v = 35$ km/s and $\theta = 30°$).

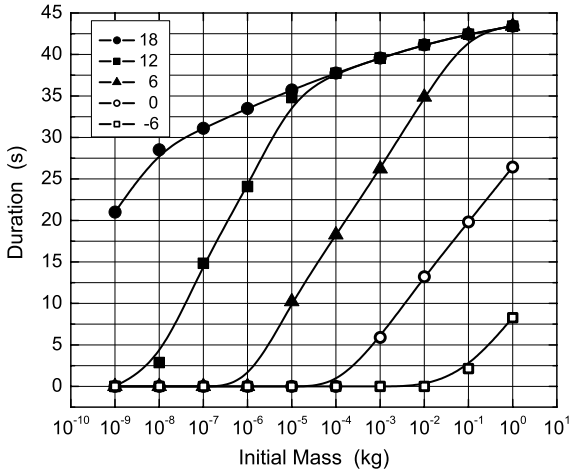

Fig. 5. – Duration of observation *vs.* the initial-mass value parameterized for the Magnitudo at threshold value $M_{\text{threshold}} = 18, 12, 6, 0, -6$ ("pure ablation process"; entry at 900 km with $v = 35$ km/s and $\theta = 30°$).

5˙2. *The numerical method.* – The combined effect of forces of drag and gravity (with the assumption of absence of lift, as stated above) in the presence of ablation results in a set of differential equations that fully describe the trajectory of a meteoroid entering the Earth atmosphere:

$$\frac{\mathrm{d}v}{\mathrm{d}t} = -C_{\mathrm{D}} \cdot \frac{\rho \cdot S \cdot v^2}{m}\,, \tag{8a}$$

$$\frac{\mathrm{d}m}{\mathrm{d}t} = -\frac{\Delta \cdot \rho \cdot S \cdot v^3}{2 \cdot \zeta}\,, \tag{8b}$$

where t, m, v, and S are, respectively, the time, mass, velocity and cross-sectional area of the meteoroid; ρ is the air density, C_{D} is the drag coefficient, ζ is the meteoroid heat of ablation and Δ is the heat transfer coefficient.

The numerical method adopted in the simulation is the "explicit forward finite difference approximation to the differential equations".

6. – Simulation parameters

The meteor simulation application has been developed in Visual C++ and it is compatible with Windows based platform. The software has a common windows graphical interface with a "wizard" (*i.e.* sequential window dialogs) initialization method which drives and facilitate the data input.

For input parameters the following numerical values have been assumed:

- *Initial meteoroid mass.* Meteoroid mass range covers several orders of magnitudes, from 10^{-9} kg, assumed as the limit mass value for micrometeorites ($\lesssim 10^{-9}$kg) and up to 10^{15} kg in the case of very large objects [10].
- *Meteoroid density.* The density range of meteoroids has been determined by studying the objects which, during the flight in the atmosphere, partially survived to the ablation and were collected as meteorites at the Earth surface. In a broad sense, meteorites can be generally classified as stone-meteorite, with reference density $\rho = 3.4$, and iron-meteorite, with density reference $\rho = 7.8$ [11].
- *Entry velocity.* The meteoroid entry velocity is determined by the combination of the solar escape velocity of an object at the Earth's orbit (42 km/s) and the orbital speed of the Earth (30 km/s). The meteoroid entry velocity is therefore set in the (12–72) km/s range.
- *Entry angle.* The range is between 90° (impact perpendicular to the atmospheric surface) and 0° (impact tangent to the atmospheric surface).
- *Entry altitude.* The impact of the meteoroid with the atmosphere has been set at 900 km above the Earth surface, considering this altitude as the limit above which the atmosphere density can be considered negligible in a friction process.
- *Heat of ablation.* The heat of ablation is a function of the material type and the specific process of ablation. An average value of $(5 \cdot 10^6)$ J/kg is commonly adopted [12, 13].
- *Heat transfer coefficient.* According to the literature a typical value of 0.01 is adopted [14-16].

TABLE I. – *Ablation only ($v = 35$ km/s, $\theta = 30°$).*

Mass (kg)	UV_{max} (M_{UV})	Altitude-UV_{max} (km)	Altitude-Start (km)	Altitude-End (km)	Track length (km)	Duration (s)
			Threshold = 18 (M_{UV})			
1	−9.02	152.34	900.00	130.98	1524.28	43.42
10^{-1}	−6.28	176.37	900.00	148.36	1490.13	42.45
10^{-2}	−3.57	199.99	900.00	171.25	1445.13	41.17
10^{-3}	−0.98	243.32	900.00	199.77	1389.02	39.57
10^{-4}	1.62	281.71	900.00	232.24	1325.12	37.76
10^{-5}	4.20	322.86	900.00	268.61	1253.49	35.72
10^{-6}	6.76	367.10	900.00	308.28	1175.27	33.50
10^{-7}	9.31	413.30	900.00	351.04	1090.88	31.10
10^{-8}	11.86	461.17	900.00	396.95	1000.20	28.52
10^{-9}	14.41	510.54	818.20	447.44	736.92	21.01
			Threshold = 12 (M_{UV})			
1	−9.02	152.34	900.00	130.98	1524.28	43.42
10^{-1}	−6.28	176.37	900.00	148.36	1490.13	42.45
10^{-2}	−3.57	199.99	900.00	171.25	1445.13	41.10
10^{-3}	−0.98	243.32	900.00	199.77	1389.02	39.57
10^{-4}	1.62	281.71	900.00	232.24	1324.97	37.75
10^{-5}	4.20	322.86	884.18	269.00	1221.07	34.80
10^{-6}	6.76	367.10	736.40	309.89	845.55	24.08
10^{-7}	9.31	413.30	620.48	357.59	520.76	14.83
10^{-8}	11.86	461.17	490.44	439.34	461.17	2.88
			Threshold = 6 (M_{UV})			
1	−9.02	152.34	900.00	130.98	1524.28	43.42
10^{-1}	−6.28	176.37	900.00	148.36	1490.13	42.45
10^{-2}	−3.57	199.99	789.87	171.32	1225.02	34.88
10^{-3}	−0.98	243.32	665.92	200.20	921.33	26.22
10^{-4}	1.62	281.71	559.22	234.35	642.16	18.27
10^{-5}	4.20	322.86	460.07	278.17	359.36	10.22
			Threshold = 0 (M_{UV})			
1	−9.02	152.34	601.44	131.01	927.87	26.43
10^{-1}	−6.28	176.37	501.96	148.72	697.09	19.82
10^{-2}	−3.57	199.99	409.21	173.47	464.88	13.22
10^{-3}	−0.98	243.32	317.84	212.44	207.76	5.90
			Threshold = −6 (M_{UV})			
1	−9.02	152.34	280.35	132.48	291.05	8.27
10^{-1}	−6.28	176.37	201.92	163.37	75.89	2.15

Note: Decimal digits derive strictly from computation and therefore they do not have necessarily "physical" relevance.

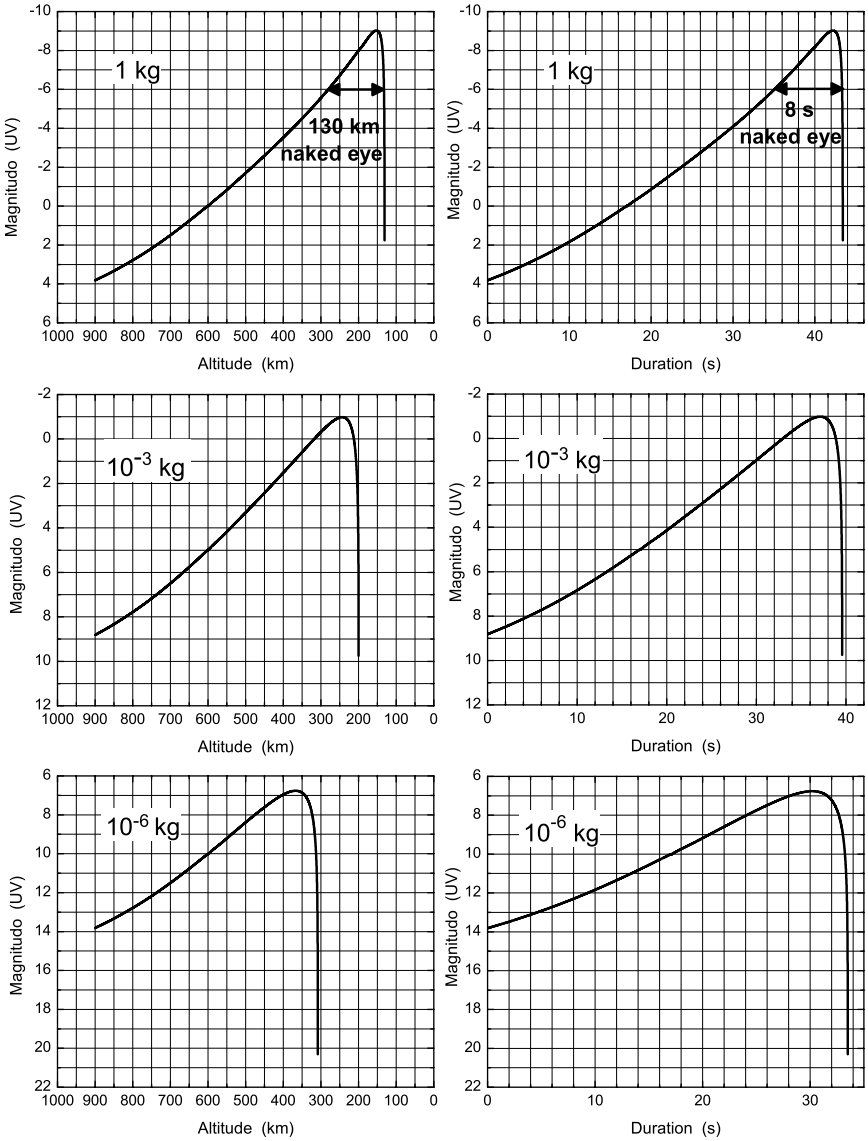

Fig. 6. – Ablation process only: $v = 35$ km/s and $\theta = 30°$. UV-Magnitudo *vs.* altitude a.s.l. and *vs.* duration for different values of the initial mass.

– *Luminosity coefficient.* $3{\cdot}10^{-4} \leq \tau \leq 2{\cdot}10^{-5}$ [5]. We have assumed $\tau = 0.01$ according to Hills and Goda [9].

– *Color Index.* To be chosen according to the spectral emission of meteors. By default Vega has been assumed as reference (*C.I.* =0.0).

– *EUSO UV threshold.* To be set according to EUSO technical specification: a numerical value of 18 has been adopted at present (B. Sacco, private communication).

– *Time calculation step.* As stated above, the accuracy of the explicit forward finite

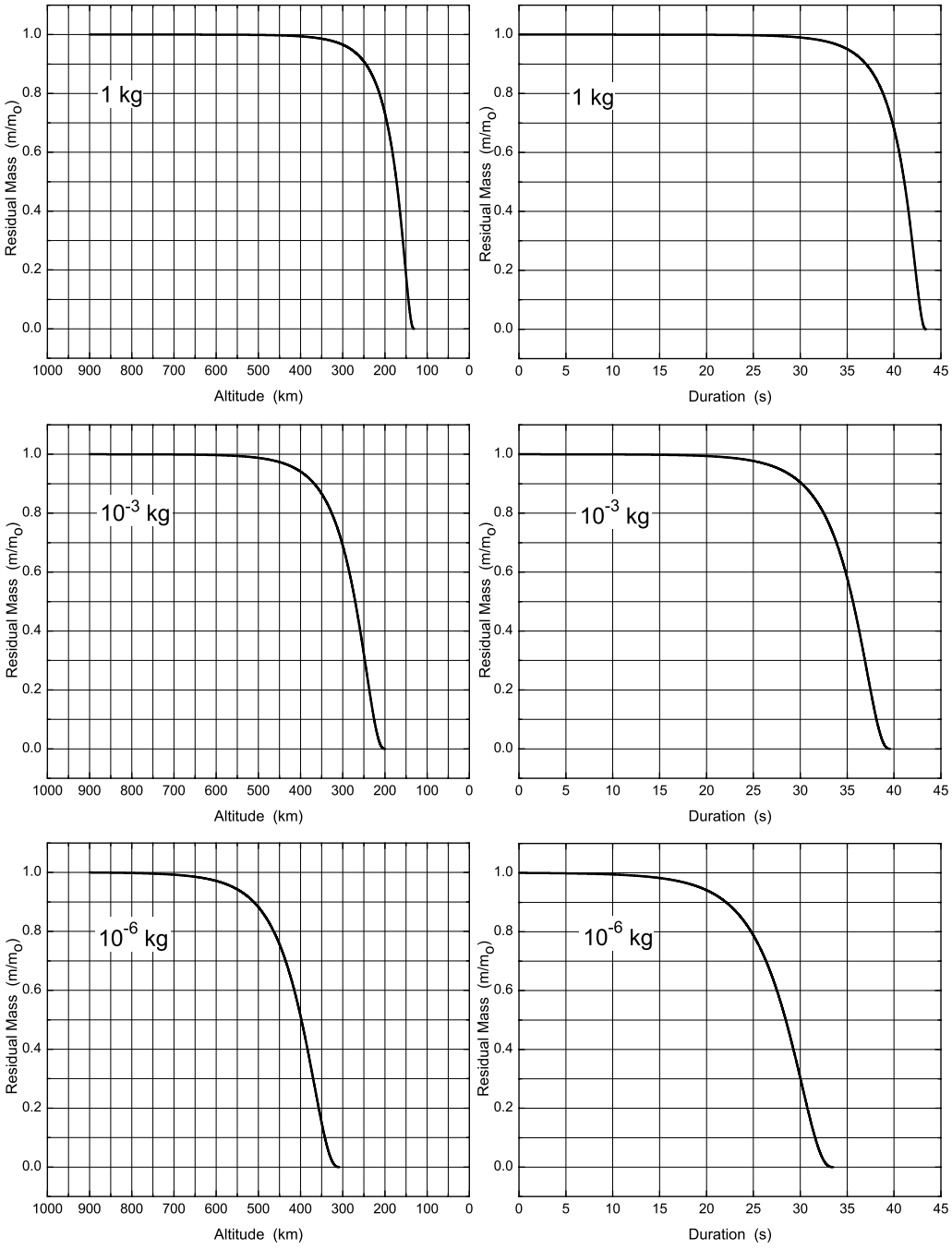

Fig. 7. – Ablation process only: $v = 35$ km/s and $\theta = 30°$. Residual mass *vs.* altitude a.s.l. and *vs.* duration for different values of the initial mass.

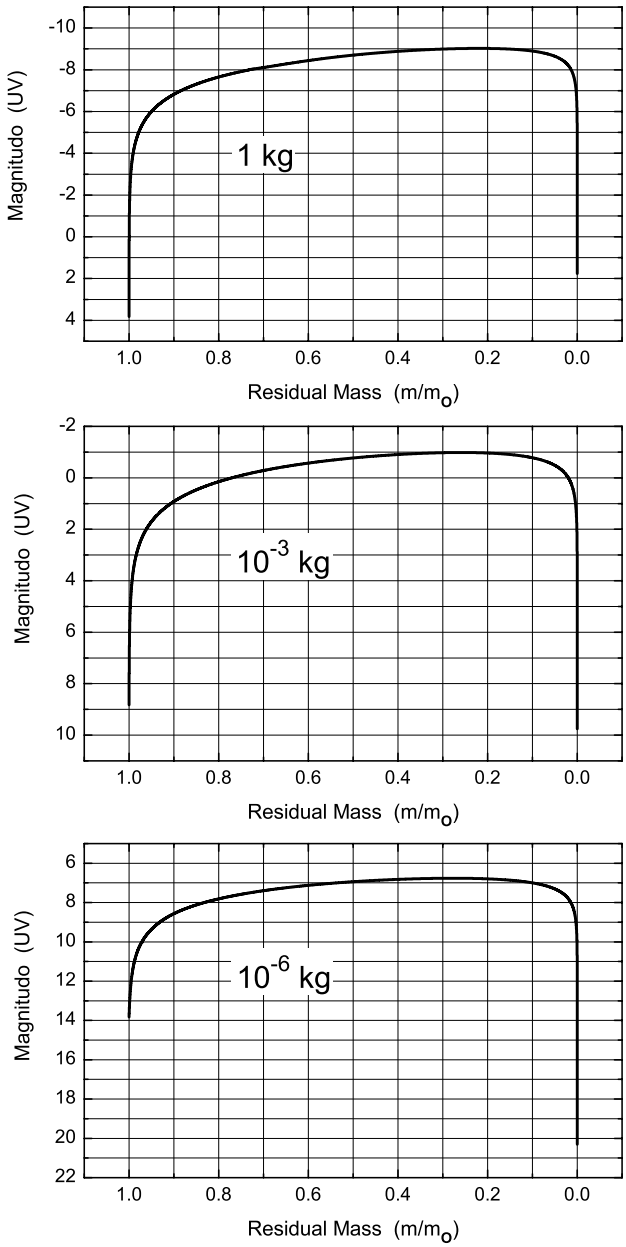

Fig. 8. – Ablation process only: $v = 35$ km/s and $\theta = 30°$. UV-Magnitudo *vs.* residual mass for different values of the initial mass.

difference method is improved by adopting smaller time increments. A control is made during the run so that the time step needs to be reduced if the meteoroid change in mass or in velocity/position is greater than a predetermined value (*e.g.*, 10%) during each interval.

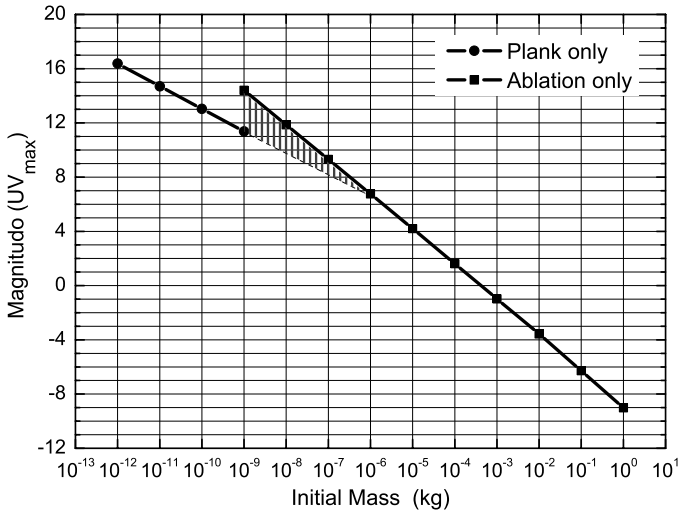

Fig. 9. – Value of the maximum value reached by the meteor UV-Magnitudo as a function of the initial mass of the meteoroid and fixed entry values: $v = 35$ km/s, $\theta = 30°$; only Plank emission from the heating process is considered for $m < 10^{-9}$ kg and only the ablation process is considered above the 10^{-9} kg limit.

7. – Meteor dependence on parametric values

The range of mass values to which the "ablation regime" can be applied is limited on the low-mass side (10^{-8}–10^{-9}) kg by the competing process of heat transfer to the interior of the meteoroid giving rise to an increase in the global temperature of the solid body reaching the melting point, with a transition to the "micrometeorite regime" with no ablation and the cooling assured by Plank radiation and the other processes of transfer to the surrounding medium (see sect. **8**).

Table I gives, as a function of the initial mass of the meteoroid, the Magnitudo corresponding to UV_{max}, the UV_{max} altitude, altitude of start and end of detectable UV emission above threshold value, track length and duration above threshold.

Figure 4 gives, at various values of threshold for the UV-Magnitudo, the start and end altitude for the observable meteor as a function of the initial-mass value.

TABLE II. – *Micrometeors ($m \leq 10^{-9}$ kg).*

Mass (kg)	UV_{max} (M_{UV})	Altitude UV_{max} (km)	Flux density (Jy)	UV photons flux (W/m^2)	UV photons (no.)
10^{-12}	16.37	103.63	$5.41{\cdot}10^{-4}$	$1.35{\cdot}10^{-15}$	$2.4{\cdot}10^{3}$
10^{-11}	14.70	102.01	$2.52{\cdot}10^{-3}$	$6.29{\cdot}10^{-15}$	$1.1{\cdot}10^{4}$
10^{-10}	13.04	83.58	$1.16{\cdot}10^{-2}$	$2.90{\cdot}10^{-14}$	$5.1{\cdot}10^{4}$
10^{-9}	11.37	79.86	$5.41{\cdot}10^{-2}$	$1.35{\cdot}10^{-13}$	$2.4{\cdot}10^{5}$

Decimal digits derive strictly from computation and therefore they have not necessarily "physical" relevance.

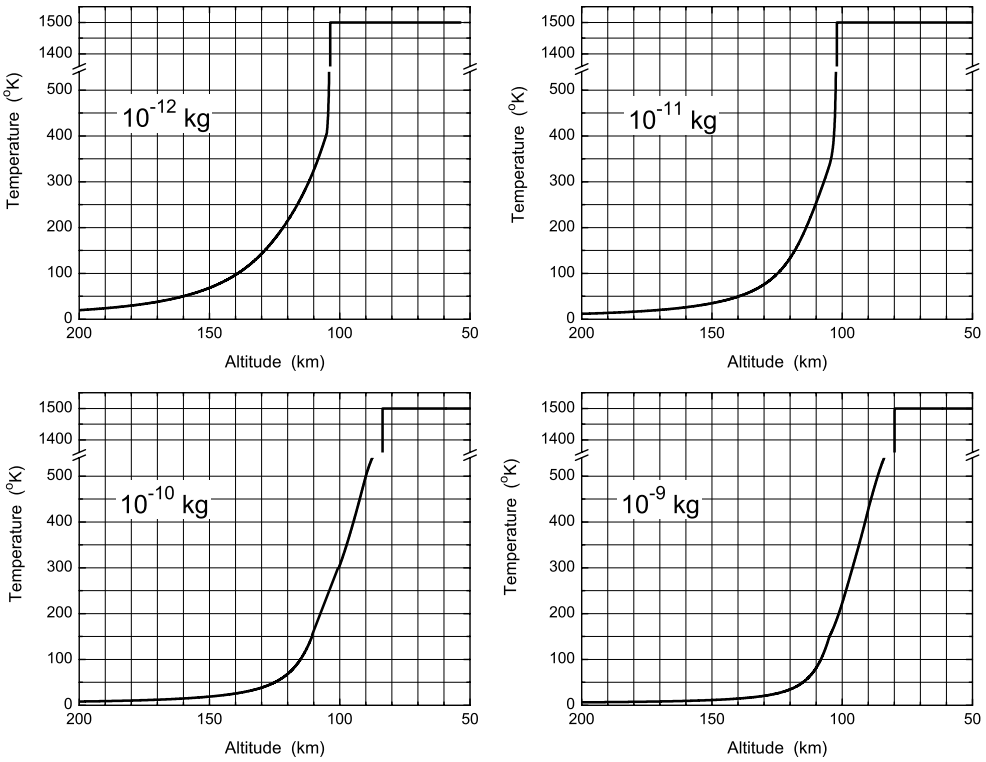

Fig. 10. – No ablation: $v = 35$ km/s and $\theta = 30°$. Temperature *vs.* altitude a.s.l. for different values of the initial mass.

As a function of luminosity threshold: at $M_{\text{UV-threshold}} = 18$ for $m_0 = 10^{-9}$ kg the observable track length is still > 400 km; at $M_{\text{UV-threshold}} = 0$ meteors are observable down to $m_0 \sim 10^{-3}$ kg; for $m_0 > 10^{-1}$ kg meteors tracks are observable at $M_{\text{UV-threshold}} = -6$ ("naked eye" equivalent in the optical band).

Figure 5 gives the duration of the observation *vs.* the initial mass value parameterized for the Magnitudo at threshold value $M_{\text{UV-threshold}} = 18, 12, 6, 0, -6$.

Figure 6 shows, as examples, results obtained for the UV-Magnitudo track profile *vs.* altitude a.s.l. and *vs.* meteor duration for some initial-mass values. The simulations show that the meteor phenomenon is on-setting already very high in the atmosphere reaching a value of $M_{\text{UV}} \sim 4$ for $m_0 = 1$ kg and a value of $M_{\text{UV}} \sim 9$ for $m = 10^{-3}$ kg at an altitude of 900 km a.s.l. As the process goes on, the luminosity increases with depth of penetration, reaching a maximum of magnitude $M_{\text{UV-max}} \sim (-9)$ at $h \sim 150$ km and maintaining a value $M_{\text{UV}} < (-6)$ for ~ 8 s between 280 km and 130 km altitude. The corresponding magnitude for an initial mass $m_0 = 10^{-3}$ kg is $M_{\text{UV-max}} \sim (-1)$ at $h \sim 230$ km and $M_{\text{UV-max}} \sim 6.8$ at $h \sim 370$ km for initial mass $m_0 = 10^{-6}$ kg.

The fall in luminosity is abrupt after maximum.

The rate of mass ablation is evaluated in fig. 7. It starts to be appreciable at ~ 300 km for $m_0 = 1$kg with a transition from 90% to 10% of the initial mass in ~ 5 s falling from 250 km to 150 km; for $m_0 = 10^{-3}$ kg, the corresponding values are: ~ 450 km,

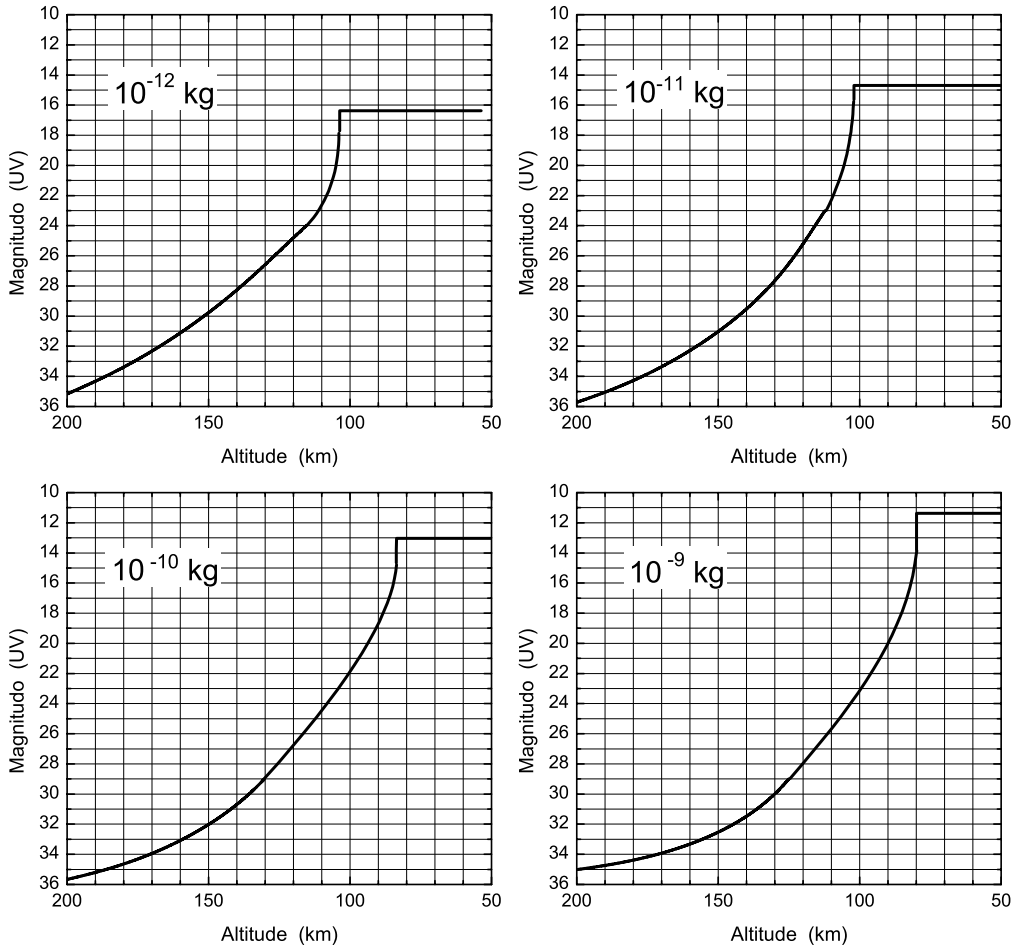

Fig. 11. – No ablation: $v = 35$ km/s and $\theta = 30°$. UV-Magnitudo *vs.* altitude a.s.l. for different values of the initial mass.

~ 8 s falling from 370 km to 220 km; for $m_0 = 10^{-6}$ kg, we find: ~ 600 km, ~ 5 s falling from 520 km to 320 km.

Figure 8 shows the UV-Magnitudo *vs.* the ratio residual/initial mass in the ablation process for initial-mass values 1 kg, 10^{-3} kg and 10^{-6}kg. The UV-Magnitudo rises abruptly for the first few percents of mass loss and drops sharply for the last few percents of the residual mass; the maximum of the curve is very broad with a peak value at about 20% of the residual-mass value.

In the different run sets described above, the initial values for the meteoroid mass are parameterized, while velocity and angle of entry and all the other quantities (C_{D}, ζ, Δ, τ, *C.I.* ...) are kept unchanged in the simulations.

Figure 9 shows with black filled squares for the pure ablation process (entry at 900 km with $v = 35$ km/s and $\theta = 30°$) the maximum value reached by the meteor luminosity, expressed in UV-Magnitudo, as a function of the initial mass in the range 10^{-9} kg to 1 kg.

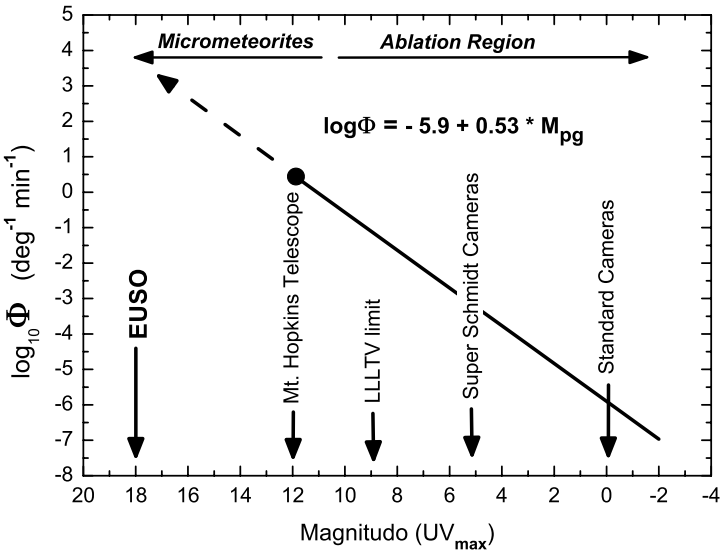

Fig. 12. – Detectable meteoroid flux *vs.* UV-Magnitudo $_{\max}$.

8. – The case of micrometeorites

For meteoroids with mass of the order of 10^{-9} kg and lower, the surface/mass ratio of the solid body increases to values consenting a surface heat dissipation rate such that the object radiates energy rapidly enough that its temperature is kept below the evaporation point and ablation does not occur. According to Whipple [17], an extraterrestrial body sufficiently small to cross the Earth's atmosphere without being destroyed and therefore to reach the ground with a residual mass (meteorite) is defined a "micrometeorite". The maximum temperature to which the micrometeorite can be heated without appreciable

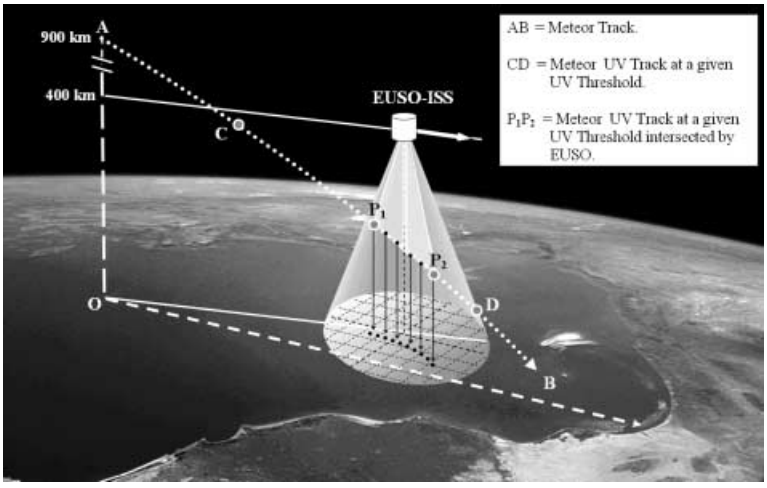

Fig. 13. – Instantaneous volume of Earth's atmosphere as observed by EUSO on the ISS.

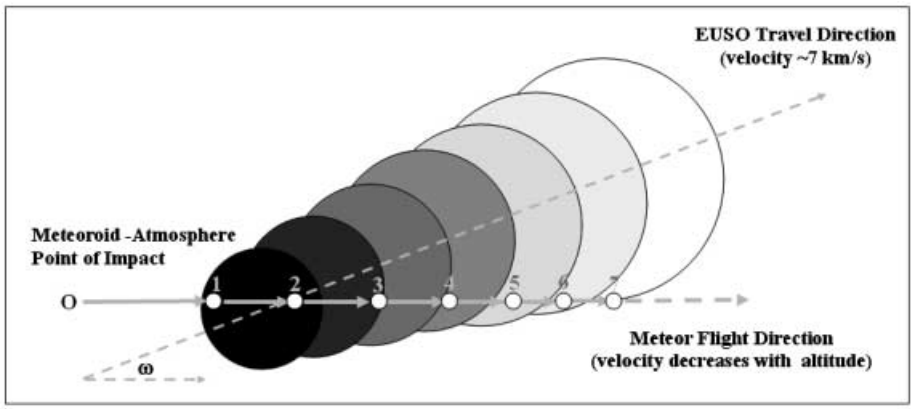

Fig. 14. – EUSO meteor observation. Different frames are taken at constant time steps Δt and are represented by sections of the "cone" with different grade of grey (first frame is heaviest, last is white). The sections move along the EUSO travel direction and are equally spaced because of the constant velocity ($\sim$ 7 km/s). The sections increase their diameter with time because they refer to progressively lower "cone-meteor" intersection altitude. The meteor velocity at each time is represented by a vector whose module decreases with time (altitude). The meteor "spot" moves with a curved trajectory on the "observation cone" projection of fig. 15.

vaporization is just below the melting point of the refractory material in the meteoroid, ranging from 1200 K to 1700 K for typical stones; iron, iron oxides and silica also fall within this range.

The simulation carried out for the light curve has considered the heat transfer to the solid body to rise its temperature near the melting point and balancing with the surface Plank radiation the energy budget for the interaction.

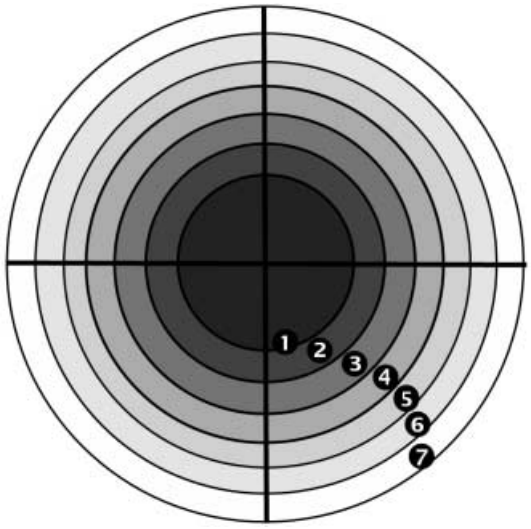

Fig. 15. – EUSO "observation cone" projection (top view). Same conventions as for fig. 13.

When the surface temperature of the meteoroid is less than its boiling point, the energy acquired per second equals the energy radiated plus the energy used to heat the meteor so that the temperature derivative is given by

$$\frac{\mathrm{d}T_\mathrm{m}}{\mathrm{d}t} = \frac{3}{r \cdot \delta \cdot c} \cdot \left[\frac{1}{8} \cdot \Delta \cdot \varphi \cdot \rho \cdot v^3 - \varepsilon \cdot \sigma \cdot \left(T_\mathrm{s}^4 - T_\mathrm{e}^4\right)\right] ; \tag{9}$$

correspondingly

$$T_\mathrm{s} = \sqrt[4]{\frac{1}{\varepsilon \cdot \sigma} \cdot \left[\frac{1}{8} \cdot \Delta \cdot \varphi \cdot \rho \cdot v^3 - \frac{1}{3} \cdot r \cdot \delta \cdot c \cdot \frac{\mathrm{d}T_\mathrm{m}}{\mathrm{d}t} + \varepsilon \cdot \sigma \cdot T_\mathrm{e}^4\right]} ,$$

where
r = meteoroid radius;
c = meteoroid specific heat;
ρ = air density;
φ = shape factor;
T_m = mean meteoroid temperature;
T_e = environmental temperature;
v = meteoroid velocity;
T_s = surface meteoroid temperature;
ε = meteoroid surface emissivity;
δ = meteoroid density;
Δ = heat transfer coefficient;
t = time;
σ = Stefan-Boltzmann constant.

Figure 10 shows the temperature *vs.* altitude profile for a meteoroid in the case of "no ablation" process with loss of kinetic energy balanced by heat transfer to the solid body resulting in no appreciable internal temperature gradient. In the range of the initial mass considered, from 10^{-12} kg to 10^{-9} kg (entry parameters assumed are $v = 35$ km/s, $\theta = 30°$), the temperature starts to increase sensibly below an altitude of about 150 km reaching a value of 1500 K at ~ 100 km for $m = 10^{-12}$ kg and ~ 80 km for $m = 10^{-9}$ kg in a time interval of about 7 s.

Figure 11 shows correspondingly the relation UV-Magnitudo *vs.* altitude; the duration of the "micrometeor" observable track by EUSO is estimated at (5–10) s before reaching ground as "micromeorite".

Table II gives the calculated UV-Magnitudo and the altitude for UV_max for micrometeoroids of mass $m = 10^{-12}$, 10^{-11}, 10^{-10}, 10^{-9} kg, density $\rho = 3.5 \cdot 10^3$ kg/m^3, temperature = 1500 K, emissivity $\varepsilon = 0.2$.

Micrometeoroids cannot be observed as "meteors" by standard optical devices (DV, cameras or LLLTV) since they do not produce a significant luminosity above the sensitivity threshold for this instrumentation. It may be assumed that the upper end of their mass range corresponds approximately to the lowest mass of a particle detectable by the most sensitive radars. Micrometeoroids are recorded mainly by detectors on spacecraft, meteoric-particle collision on rockets and balloons and collections on sea-beds and glacial deposits. As yet none of these methods enables the determination of micrometeoroids orbits; their mass distribution can be determined fairly reliably but in calculations of micrometeoroids streams the different methods show an error spread over four orders of

magnitude. EUSO, with his high sensitivity (UV-Magnitudo up to ~ 18) and signal/noise ratio is expected to be able to provide a significant direct "micrometeor" observation.

Figure 9 shows the behavior of the "UV-Magnitudo *vs.* initial-mass dependence simulated by the Plank emission (no ablation) process active below the 10^{-9} kg initial-mass limit and by dominating ablation above $m = 10^{-9}$ kg. The two regimes appear presenting a smooth transition from "radiation" to "ablation"; a mixing of the two processes is expected to occur in the boundary region.

9. – Observational range

Meteor observational sensitivity for EUSO compared to other common standard techniques is shown in fig. 12. Data for Mt. Hopkins are after [4].

10. – Data retrieval and approach to the analysis

EUSO will observe the portion of the meteor below the altitude of 400 km (see fig. 13). The trajectory of a solid body traveling in the atmosphere and intersecting the cone of observation of EUSO will determine a UV profile projected as a "track" on the instrument focal surface. The observation is photometric (no spectroscopy) with high-frequency sampling in time and position. The data retrieved can be exploited in the context of the so-called "integral light" approach of investigation. They will be the result of meteor UV emission whatever the physical process responsible.

The observation of the meteor "integral UV-light", besides tracking the meteoroid trajectory and dynamics will allow reconstructing the solid-body initial entry mass and its mass variation along the trajectory. The focal surface track is a complex function of several parameters, both instrumental and solid-body dependent. Figures 14 and 15 show an example of a meteor track as seen on the focal surface. The vector velocity of the meteoroid can be inferred by the *shape* of the track by subtracting the constant ISS vector velocity (7 km/s). Track progression velocity, the geometry and intensity of the UV-signal will provide a powerful tool for a detailed reconstruction of the meteor UV light curve.

The EUSO experiment is able to measure directly the micrometeoroid flux before atmospheric entry and it will provide an important contribution to our knowledge of this component of interplanetary solid object. Additional data and an expanded version of the simulation can be found in [18, 19].

* * *

I wish to thank the colleagues of the EUSO Team in Palermo for comments and discussions.

REFERENCES

[1] *Satellite Argos at H=833Km, Leonid maximum 18 November 1999*, NRL Report (2000).
[2] Ceplecha Z., Borovicka I., Elford W. G., Revelle D. O., Hawkes R. L., Porubcan V. and Sinek M., *Space Sci. Rev.*, **84** (1998) 327.
[3] Various Authors, *EUSO Report on the Phase A Study*, EUSO-PI-REP-005, Issue 1 (2004).
[4] Cook A. F., Weekes T. C., Williams J. T. and O'Mongain E., *Mon. Not. R. Astron. Soc.*, **193** (1980) 645.

[5] Bronshten V. A., *Physics of Meteoric Phenomena* (D. Reydel Publication Co.) 1983.
[6] *U.S. Standard Atmosphere, 1976* (US Government Printing Office, Washington D.C.) 1976.
[7] Hedin A.E, *J. Geophys. Res.*, **96** (1991) 1159.
[8] Allen C. W., *Astrophysical Quantities* (Athlone Pub.) 1973.
[9] Hills J. G. and Goda M. P., *Astron. J.*, **105** (1993) 1114.
[10] Ceplecha Z., *Astron. Astrophys.*, **263** (1992) 361.
[11] Grimmer G., *J. Appl. Phys.*, **19** (1948) 947.
[12] Baldwin B. and Shaeffer Y., *J. Geophys. Res.*, **76** (1971) 4653.
[13] Passey Q. R. and Melosh H. J., *Icarus*, **42** (1980) 211.
[14] Allen H. J., Seiff A. and Winovich W., *NASA Technical Report TR R-185* (NASA, Washington D.C.) 1963.
[15] Liu V. C., *Geophys. Res. Lett.*, **5** (1978) 309.
[16] O'Keefe J. D. and Ahrens T. J., *Geological implications of impact of large asteroids and comets on the Earth*, in *Geol. Soc. Am. SP 190*, edited by Silver L. T. and Schultz P. H. (1982), pp. 103-120.
[17] *The Collected Contributions of Fred L. Whipple—Volume One: Meteors and Comets and the Interplanetary Complex* (Smithsonian Astrophysical Observatory, Cambridge, Mass.) 1950.
[18] Scarsi P., *Meteor Observation by EUSO. From Meteoroids to Meteors: the general process, EUSO-SIM-REP-008-1* (2003).
[19] Scarsi P., *Meteor Observation by EUSO: general overview and scientific objectives, EUSO-SDA-REP-013-1* (2002).